CCFE
CULHAM CENTRE FOR FUSION ENERGY

UK Atomic Energy Authority

UKAEA-CCFE-CP(19)28

N. Vianello, D. Carralero, C. K. Tsui, V. Naulin, M. Agostini, J. Boedo, B. Labit, C. Theiler, D. Aguiam, S. Allan, M. Bernert, S. Costea, I. Cziegler, H. De Oliveira, J. Galdon-Quiroga, G. Grenfell, A. Hakola, C. Ionita, H. Isliker, A. Karpushov, J. Kovacic, B. Lipschultz, R. Mauriozio, K. McClements et al

Scrape off layer (SOL) transport and filamentary dynamics in high density tokamak regimes

Scrape off layer (SOL) transport and filamentary dynamics in high density tokamak regimes

N. Vianello, D. Carralero, C. K. Tsui, V. Naulin, M. Agostini, J. Boedo, B. Labit, C. Theiler, D. Aguiam, S. Allan, M. Bernert, S. Costea, I. Cziegler, H. De Oliveira, J. Galdon-Quiroga, G. Grenfell, A. Hakola, C. Ionita, H. Isliker, A. Karpushov, J. Kovacic, B. Lipschultz, R. Mauriozio, K. McClements et al

This paper has been submitted to
27th IAEA Fusion Energy Conference, Ahmedabad, India, 22-27 October 2018

SCRAPE OFF LAYER (SOL) TRANSPORT AND FILAMENTARY DYNAMICS IN HIGH DENSITY TOKAMAK REGIMES

N. VIANELLO[1], D. CARRALERO[2, 3], C. K. TSUI[4, 5], V. NAULIN[6], M. AGOSTINI[1], J. BOEDO[4], B. LABIT[5], C. THEILER[5], D. AGUIAM[7], S. ALLAN[8], M. BERNERT[3], S. COSTEA[9], I. CZIEGLER[10], H. DE OLIVEIRA[5], J. GALDON-QUIROGA[11], G. GRENFELL[1], A. HAKOLA[12], C. IONITA[9], H. ISLIKER[13], A. KARPUSHOV[5], J. KOVACIC[14], B. LIPSCHULTZ[10], R. MAURIZIO[4], K. MCCLEMENTS[8], F. MILITELLO[8], J. OLSEN[6], J. J. RASMUSSEN[6], T. RAVENSBERGEN[16], H. REIMERDES[5], B. SCHNEIDER[9], R. SCHRITTWIESER[9], M. SPOLAORE[1], K. VERHAEGH[10], J. VICENTE[7], N. WALKDEN[8], W. ZHANG[3], E. WOLFRUM[3], the ASDEX-Upgrade Team[3], the TCV team[17] and and the EUROfusion MST1 Team[18]

[1] *Consorzio RFX, Padova,Italy,* [2]*CIEMAT Laboratorio Nacional de Fusión, Madrid, Spain,* [3]*Max-Planck-Institut für Plasmaphysik, Garching, Germany,* [4]*EPFL-SPC, Switzerland,* [5]*UCSD, La Jolla, USA,* [6]*DTU, Lyngby, Denmark,* [7]*IPFN, Instituto Superior Técnico, Lisboa, Portugal,* [8]*CCFE, Culham, UK,* [9]*Institute for Ion Physics and Applied Physics, Innsbruck, Austria,* [10]*York Plasma Institute, University of York, UK,* [11]*University of Seville, Seville Spain,* [12]*VTT, Espoo, Finland,* [13]*Aristotle University of Thessaloniki, Greece,* [14]*Jozef Stefan Institute, Ljubljana,* [16]*DIFFER—Dutch Institute for Fundamental Energy Research, Netherlands,* [17]*See the author list S. Coda et al 2017 Nucl. Fusion 57 102011,* [18]*See the author list H. Meyer et al 2017 Nucl. Fusion 57 102014*

Corresponding Author: nicola.vianello@igi.cnr.it

Abstract:

A detailed cross-device investigation on the role of filamentary dynamics in high density regimes has been performed within the EUROfusion framework comparing ASDEX-Upgrade (AUG) and TCV tokamaks. Both devices have run density ramp experiments at different levels of plasma current, keeping toroidal field or q_{95} constant in order to disentangle the roles of parallel connection length and the current. In both devices, with constant toroidal field, SOL profiles tend to flatten at lower edge density whenever current is reduced even though the behavior is reconciled in terms of Greenwald fraction whereas the runs at constant q_{95} exhibit unclear results whenever both devices are considered. ASDEX-Upgrade has also explored the filamentary behavior in inter-ELM regimes in H-Mode. The experiments on AUG focused on the role of neutrals, performing discharges both with and without the cryopumps, highlighting the how large neutral pressure not only in the divertor but at the midplane is needed in order to develop H-Mode SOL profile shoulder in AUG. Finally particle acceleration during the eruption of ELM filaments has been investigate in order to understand possible impact on Plasma Facing Components of of fast accelerated electron and ions in the SOL.

1 INTRODUCTION

Plasma Wall Interaction (PWI) is a subject of intense study in the context of fusion energy research for the understanding of the amount of heat loads, tritium retention, and the lifetime of different Plasma Facing Components. In recent years great efforts have been devoted to the interpretation of Scrape Off Layer (SOL) transport, with clear impact also on the design of future machines [1]. Transport in the SOL region, resulting from a competition between sources and parallel and perpendicular losses, is dominated by the presence of intermittent structures, filaments, which strongly contribute to particle and eventually energy losses both in L- and H-mode regimes. The role of convective radial losses has become even more important due to its contribution to the process of profile broadening also known as *shoulder formation* in L-Mode, describing the progressive flattening of the density scrape off layer profile at high density [2–6] where future devices are expected to routinely operate. This increased radial transport could pose serious problems for Plasma Facing Components. Preliminary investigations suggested that similar mechanisms occur in H-Mode as well [7–10] and that filaments strongly contribute to power balance and SOL transport also in the so-called H-mode density limit (HDL) [11, 12]. The present contribution will report results of a coordinated effort within the EUROfusion Medium Sized Tokamaks (MST1) framework between the ASDEX-Upgrade (AUG) and TCV tokamaks, to address the role of filamentary transport in high density regimes both in L- and H-Mode. The combined results allow the comparison, using similar methodology and techniques, of the results obtained in largerly different devices from a machine with a closed divertor, metallic first wall and cryogenic pumping system, to a carbon machine with a completely open divertor. The mechanism of shoulder formation and the role of filamentary transport have been tested against variations of plasma current and parallel connection length, and divertor neutral densities in H-Mode, through modification of cryopump efficiency.

2 CURRENT SCAN

The first set of experiments consisted of a series of density ramps, up to disruption, at different levels of current but keeping the same toroidal field on a shot-to-shot basis. The typical plasma parameters are shown in Fig.1I for both devices. The first clear observation is the differences in parallel connection length $L_{||}$ shown as the length from the target up to the height of the X-point, which clearly demonstrate the larger $L_{||}$ obtained in TCV. The density ramps were performed by keeping the edge density between different currents comparable. In Fig 1II the same quantities are shown for a similar current scan where the toroidal field has been changed together with current to keep a

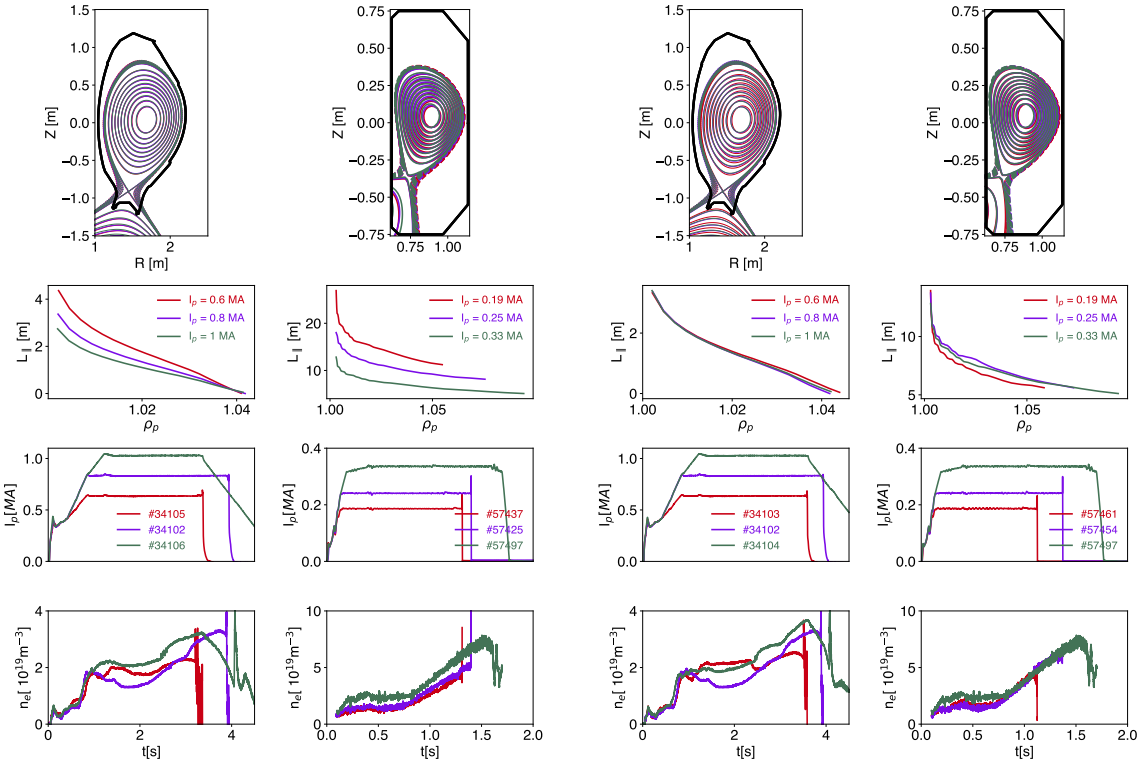

(I) Current scan at constant B_t *(II) Current scan at constant q_{95}*

FIG. 1: Main plasma parameter during current scan. In both the figures the left column refers to ASDEX-Upgrade experiments, the right one to TCV. In each plot we show from top to bottom: plasma equilibria, the parallel connection length $L_\parallel$ from the target to the height of the X-point as a function of normalized poloidal flux, the plasma current and the edge density from interferometer measurement.

constant q_{95} on a shot-to-shot basis. In this case the parallel connection length is kept approximately constant at the different current levels, with some small difference for TCV at lower current: it is worth mentioning that in TCV the toroidal field used at lower current is unusually low for this device ($B_t \approx 0.8$T).

Fig. 2 shows the peak target density and the radiation as obtained from Line of Sight (LoS) looking close to the target as a function of density for both the machines obtained during the current scan at constant toroidal field and at constant q_{95} respectively in subfigures 2I and 2II.
During the constant B_t scan clearly plasma detached at larger density for higher current for both the machines. It is worth noting the different behavior of the two devices: as already noted [13] the peak density in TCV increases almost linearly for all the cases up to the threshold followed by a smooth rollover. In ASDEX-Upgrade on the other hand the increase of density is faster than linear up to the threshold with a more pronounced rollover. These differences are likely due to different divertor closure [14], with increased radiative and charge exchange losses in

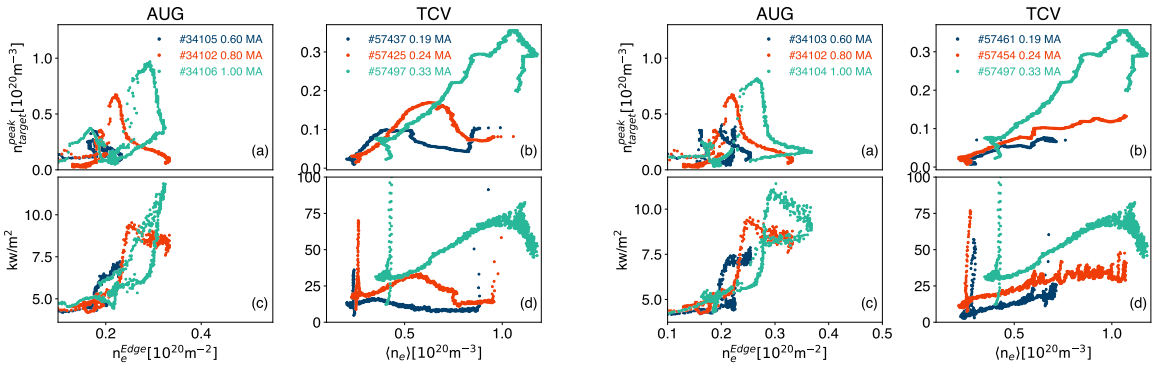

(I) Current scan at constant B_t *(II) Current scan at constant q_{95}*

FIG. 2: Panels (a): peak target density in AUG as a function of line-integrated edge density. Panels (b): peak target density in TCV as a function of central chord density. Radiation from LoS looking at the target as a function of line average density (panels (c)) and average density from central chord (panels (d)). Radiation obtained from AXUV diagnostic in ASDEX-Upgrade and Bolometry for TCV.

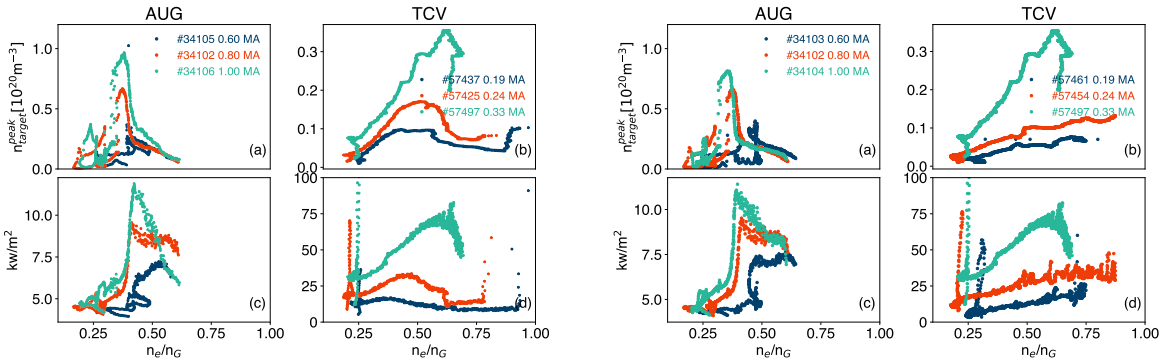

(I) Current scan at constant B_t *(II) Current scan at constant q_{95}*

FIG. 3: Peak target density as a function of Greenwald fraction for the different current values (panels (a) and (b)). Radiation from LoS looking at the target as a function of Greenwald fraction (panels (c) and (d)). In all the panels the Greenwald fraction is computed considering the central density.

closed divertor due to an enhancement in neutrals trapping.

During the scan at constant q_{95}, (shown in Fig 2II) the target evolution for ASDEX-Upgrade follows a similar behavior with a classical transition to highly recycling, rollover and detachment. For TCV on the other hand whenever the current is reduced, both the peak target and the radiation exhibit a linear increase with no signature of detachment. Recently the process of ion flux rollover in TCV has been investigated both experimentally [15] and numerically [16] in TCV: it has been found that divertor target ion current loss is driven by a reduction in the power available for ionization, a process known as *power starvation*: this process is likely not to happen at lower current during the q_{95} sacn. The same analysis can be performed as a function of normalized Greenwald fraction as shown in Fig 3I and 3II. This analysis seems to reconcile the different currents explored for the scan at constant toroidal field in AUG: in this device the rollover happens between 0.3 and 0.4 in Greenwald fraction for AUG, which are values typical for closed divertor devices, whereas it happens at higher normalized density for TCV where differences between the different currents remain.

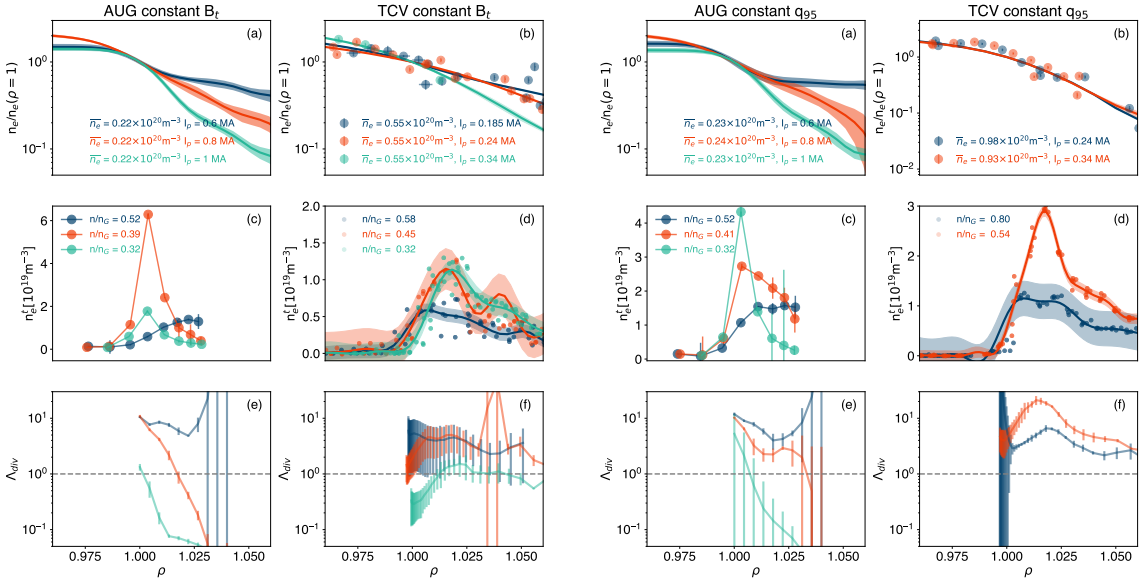

(I) Current scan at constant B_t *(II) Current scan at constant q_{95}*

FIG. 4: Top panels: SOL uptream profiles, normalized to values at the separatrix for 3 different currents at the same edge density. Middle panels: Target density profiles. Bottom panels: Λ_{div} profiles

When q_{95} is kept constant, the differences between the different current levels remain also for AUG with rollover observed at lower Greenwald fraction at higher current. The reason for this is presently unclear and under investigation. In correspondence with the increased fueling and target evolution the upstream profiles are modified as well. The evolution of upstream profiles at similar values of edge density for the two current scans are shown

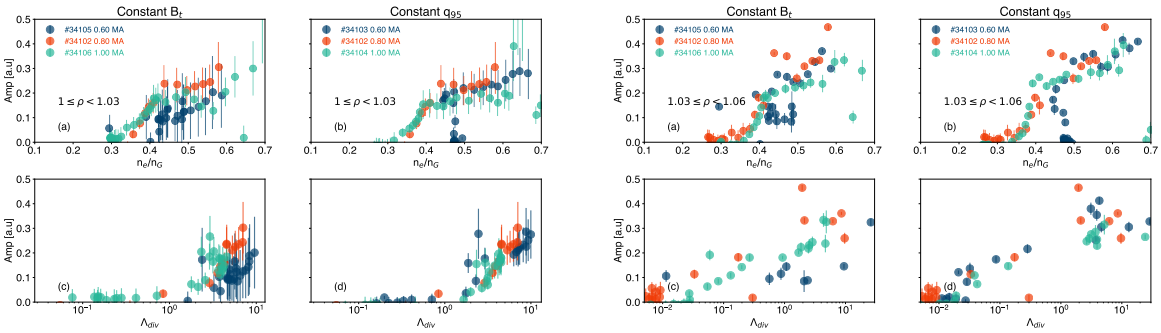

(I) Shoulder amplitude in the near SOL *(II) Shoulder amplitude in the far SOL*

FIG. 5: Shoulder amplitude as a function of Greenwald fraction for different currents levels in the constant B_t (panels (a)) and constant q_{95} (panels (b)) respectively in the near SOL (subfigure (a)) and far SOL (subfigure (b)). Shoulder amplitude as a function of Divertor collisionality Λ_{div} for different currents levels in the constant B_t (panels (c)) and constant q_{95} (panels (d)) respectively in the near SOL (subfigure (a)) and far SOL (subfigure (b)). Only ASDEX-Upgrade data are shown.

in Figures 4I and 4II respectively. In the top panels of Figures 4 the SOL density profiles normalized to values at the separatrix are shown for the same level of density at different currents. Clearly for the scan at constant toroidal field (cf. Figure 4I) flatter profiles are obtained at lower currents both for AUG and for TCV. The data shown has been obtained from Li-BES in AUG, whereas a combination of Thomson scattering and Reciprocating langmuir probe [17] allowed the reconstruction of density profile in TCV. The line showed in panels (b) of subfigures 4I and 4II are obtained from gaussian process regression (GPR) fit, whereas the symbols indicate the experimental data. This is also associated to different divertor conditions, which exhibit broader target density profiles at lower current as shown in panels (c) and (d) of subfigures 4I and 4II. The lines shown in panels (d) refer to a GPR fit performed on the data shown as symbols. In the same figures in the bottom rows we report the profile of the divertor collisionality $\Lambda_{div} = \frac{L_{\parallel}\nu_{ei}}{c_s}\frac{\Omega_i}{\Omega_e}$ originally introduced in [18] and adopted in [4] as a parameter to identify enhanced filamentary transport transition in high density regimes. We can indeed confirm from the scan reported in Fig. 4I that flatter profiles (blue curves in panel (a)) are observed for higher values of Λ_{div} all along the profiles and this observation holds strongly for ASDEX-Upgrade. On the other hand considering Fig. 4II with the scan at constant q_{95} no modifications of upstream profiles are observed for TCV and this is true even though the Λ_{div} profiles are well above 1 all along the profiles. This is consistent with observation reported in [6] which clarified that high values of divertor collisionality are insufficient to guarantee robust upstream modifications in TCV, observed only with pronounced detachment not achieved in the present scan. An alternative method to provide a quantitative description of the evolution of upstream profiles, *the shoulder amplitude*, has been introduced in [19]: the amplitude is defined as the difference between normalized upstream profiles with respect to a reference profile in the sheath limited regime (taken as the average profile in a 200 ms time at the beginning of the flat top before the fueling ramp). The evolution of the mean amplitude in the near and far SOL, defined as the regions before and after the value of $\rho_p = 1.03$, are shown in figures 5I and 5II respectively for ASDEX-Upgrade. The points represent the average values in the aforementioned spatial regions and computed as a running mean over 80ms, whereas the error bars indicate the running standard deviation. The main observation is that the evolution in the near and far SOL are actually very similar for both the scans: upstream profiles starts evolving in the near SOL for normalized Greenwald fraction around 0.35, corresponding to the transition to high recycling regime consistently with observation obtained in horizontal target configuration in JET [19]. Panels (c) and (d) of Figures 5I and 5II show the dependence of the shoulder amplitude from the divertor collisionality the latter computed as an average value in the near ($1 \le \rho < 1.03$) and far ($1.03 \le \rho < 1.06$) SOL: the results confirm the utility of Λ_{div} as a parameter for characterizing the evolution of upstream profile in all the explored conditions in ASDEX-Upgrade, as pointed out in [9].

2.1 Influence of neutrals in shoulder formation

Even though the increase of filamentary convective transport has been recognized since the beginning [3] to play a fundamental role in the process of shoulder formation, the role of other mechanisms is presently under consideration. Among them the influence of neutrals in the divertor region, which has been theoretically proposed [20] and experimentally suggested in [19] is the subject of intense study. On the other hand also the role of neutrals in the main chamber which could modify the ionization rate in the Outer Midplane (OMP) has been proposed as a possible candidate in the process of shoulder formation [9], even though it is still debated [5]. This motivated an experimental activity to analyze Balmer emission profiles in ASDEX-Upgrade by means of a D_α calibrated camera. The camera is looking almost tangentially into the main chamber and inverted emission profiles, limited to the divertor region, are obtained using the SART technique [21], without any input from the equilibrium or regularization. At the beginning emission is strongly localized in the inner divertor (see Figure 6), consistent with the

presence of a High Field Side high density region [22, 23].

During the fueling ramp the divertor moves into a high recycling regime and D_α radiation moves towards the low field side (LFS) region, initially in the private flux region (PFR) and then in the main SOL moving upstream once the target density rolls over.

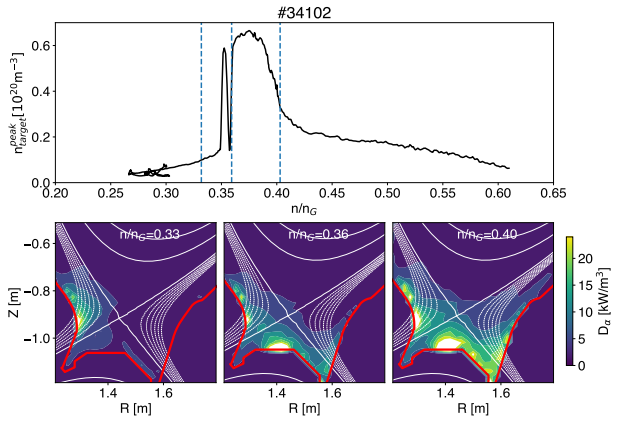

FIG. 6: Top: Peak target density vs greenwald fraction. Bottom: Tomography inversion of D_α radiation from calibrated CCD camera at three different time instants marked with vertical lines in the upper panel. Only ASDEX-Upgrade data are presented

This strongly resembles the observation on JET in the Horizontal Target [19]: in this configuration indeed the upstream profile develops a clear shoulder whenever fueling is raised, and this is accompanied by a clear D_α radiation front moving into the main LFS SOL. On the other hand whenever run in the Vertical Target configuration no shoulder is observed in JET at the same level of fueling, and D_α radiation was confined to a narrow region along the divertor leg. This observation then seems to reconcile the behavior of JET and ASDEX-Upgrade despite the different divertor configuration

2.2 Filaments characteristics

The role of enhanced convective filamentary transport in the formation of SOL density shoulder has been already suggested [3, 4, 6], even though reduced parallel losses could also influence the processes. The relation between profile evolution and blob-sizes has been investigated in the present scan using properly designed probe arrays with methodology described in [24] and [17] for AUG and TCV respectively. It is worth noting that we are considering δ_b as the radius of the blobs, differently from [4, 6] where blob diameter was shown.

The results are shown in figures 7I where the e-folding length $\lambda_n = (\frac{|\nabla n_e|}{n_e})^{-1}$ is shown as a function of blob-size shown in ion-sound gyroradius units. The latter is computed as $\rho_s = \frac{c_s}{\Omega_i}$: for TCV local electron temperature is used and the assumption $T_e = T_i$ is considered. For ASDEX-Upgrade no local T_e was available for the present scan and thus we rely on the assumption of $T_e = 15$ eV and $T_i = 3T_e$ for $\Lambda_{div} \lesssim 1$ and $T_i = T_i$ otherwise, as reported in [25]. This implies an average value of 0.7mm for TCV and 0.58 and 0.4 for AUG respectively at low and high collisionality. The reported λ_n is computed at the same radial location of the blobs, approximately at $1.03 \lesssim \rho \lesssim 1.05$. The increase of e-folding length, or equivalently the flattening of the profile is correlated to the increase of filament blob-size for the constant toroidal field scan for ASDEX-Upgrade, whereas the relation is less robust for TCV as testified by the R^2 coefficient of the power law fit reported in the panels (a) and (c) of subfigure 7I. During the scan at constant q_{95} shown in the same Figure 7I (panels (b) and (d)), ASDEX-Upgrade confirms this relation whereas the e-folding length remain basically constant for TCV with a limited variation of the blob-size.

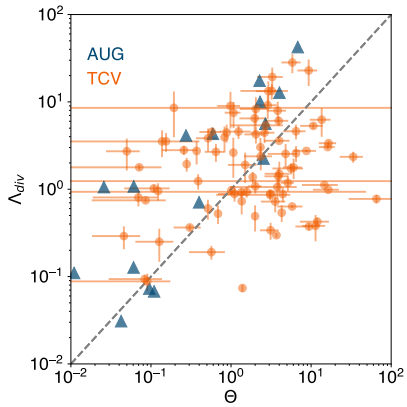

FIG. 8: Λ_{div} vs Θ for L-Mode discharges in TCV and ASDEX-Upgrade

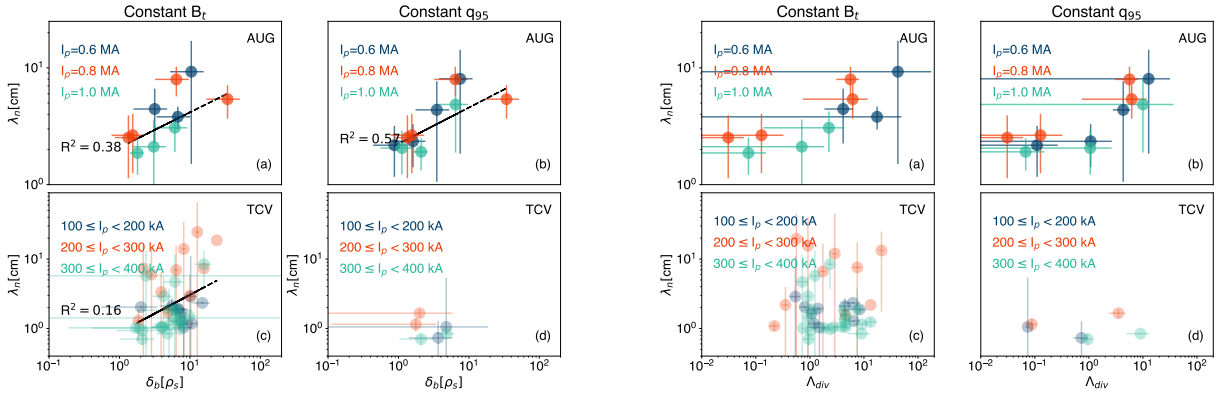

(I) λ_n vs blob-size *(II) λ_n vs Λ_{div}*

FIG. 7: E-folding length as a function of blob-size δ_b (left) and as a function of divertor collisionality Λ_{div} (right)

The evolution of λ_n has been analyzed also as a function of divertor collisionality as shown in Figure 7II.

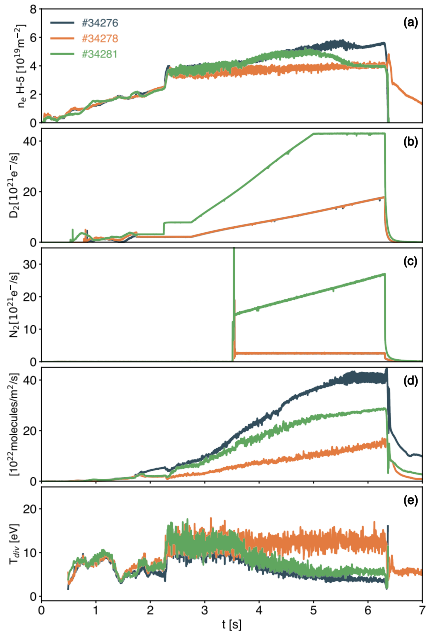

FIG. 9: (a) Edge density (b) Total deuterium fueling (c) Total nitrogen seeding (d) Subdivertor neutral pressure (e) Divertor temperature for 3 H-mode discharges. Only ASDEX-Upgrade data are presented

The already proved sharp increase of λ_n above $\Lambda_{div} \gtrsim 1$ is confirmed for ASDEX-Upgrade for both scans independently on the current, whereas from the scan at constant q_{95} we confirm that an increase of Λ_{div} does not imply necessary upstream profile flattening on TCV, since the e-folding length remains constant over a wide variation of divertor collisionality. This is consistent with the fact that the divertor remains attached in TCV as shown in Fig. 5II. In [4] it has been argued that the appearance of shoulder is related to a transition from sheath-limited to inertial regimes causing a modification of the size-velocity scaling. The paradigm adopted is based on the theoretical framework introduced in [18] which describes the blob properties in the plane $\Theta - \Lambda$ where Λ has been already introduced and $\Theta = \left(\frac{\delta_b R^{1/5}}{L_\parallel^{2/5} \rho_s^{4/5}} \right)^{5/2}$ is a normalized blob-size. Figure 8 summarizes the blob description for the two devices. As pointed out already in [17] TCV blobs have features consistent with a resistive interchange baloooning type. Surprisingly for the shots analyzed, ASDEX-Upgrade exhibits similar behavior, although we need to underline the uncertainty arising from the lack of local temperature information. If considered in the framework of aforementioned two-region blob proposed in [18], this would mean that the filaments are always disconnected from the divertor plate, even at lower collisionality with marginal increase of the velocity. Presently work is in progress to obtain velocity information from independent measurements, as fast camera velocimetry measurements, which will give us additional data to support or disprove these considerations. In any case this observation, although preliminary, suggests that the different behavior of the two devices must reside on different mechanism, as neutral distribution or different SOL opacity [9].

3 H-MODE SHOULDER FORMATION

The question of whether the mechanism of SOL profile flattening is affecting also the inter-ELM profiles in H-Mode is a fundamental issue, since operation at high Greenwald fraction with divertor in detached condition is envisaged for future reactor-relevant plasmas.

In the present contribution previous work described in [9, 10] has been extended by detailed filamentary investigations in AUG in a relatively high power discharges focusing on the role of divertor neutral pressure by comparing operation with and without the cryopumps. The time traces of relevant parameters are shown in figure 9 for 3 different discharges at 0.8MA, B_t = -2.5T in ASDEX-Upgrade all with the same heating power of 5.6 MW obtained through a combination of NBI and ECRH. Shots # 34276 and 34278 were operated with the same fueling and seeding settings without and with the cryopumps, whereas for shot # 34281, where the cryopump was operated, both fueling and seeding were increased with the aim of matching the subdivertor neutral pressure (panel (d) of Figure 9). It is worth noting that the level of fueling attained in these shots is much higher than what reported in [9]. Comparing shots #34276 with #34278 we observe that keeping the same level of fueling and seeding but starting the cryopump prevents the plasma from detachment (indicated by constant divertor temperature) with a modest increase in edge density. To reach similar conditions for edge density and detachment, very high level of fueling and seeding are needed, even though we note that

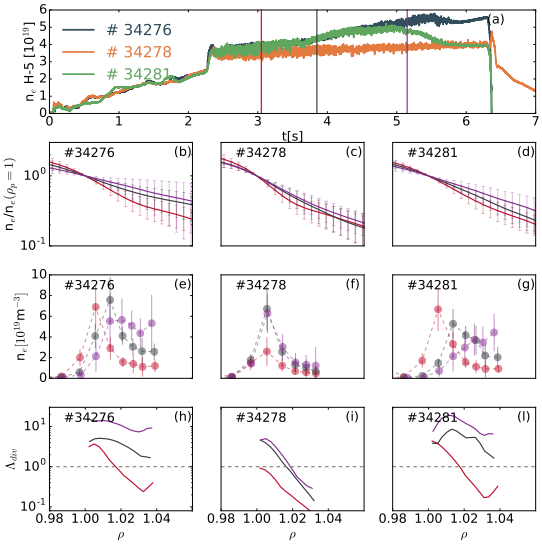

FIG. 10: Edge density vs time for the shots #34276, #34278 and #34281 (a). Inter-ELM upstream density profiles normalized to values at the separatix (b-d). Target density profiles (e-g), Λ_{div} profiles (h-l). In (b-l) colors refer to the time instants marked in (a). Only ASDEX-Upgrade data are presented

HDL is attained earlier in density for shot 34281, as shown by the rollover of edge density at 5s. In Figure 10 the upstream and target inter-ELM profiles for the same three shots are shown for three different time instants. In all cases we start from a clearly attached plasma with a steep upstream profile and a divertor collisionality completely, or at least partially, below the threshold $\Lambda_{div} = 1$. Both the target and upstream profiles start evolving for shots with comparable subdivertor neutral pressure (# 34276 and # 34281) moving towards high recycling and finally to fully detached conditions. Consistently the divertor becomes fully collisional with a Λ_{div} profile well above 1 in all the explored radial region and the upstream profiles tend to flatten. On the other hand for shot #34278 the upstream and target profiles remain practically unchanged with the peak target density still increasing without sign or roll-over. This is true even though Λ_{div} increases in the near SOL. Filament characteristics have been investi-

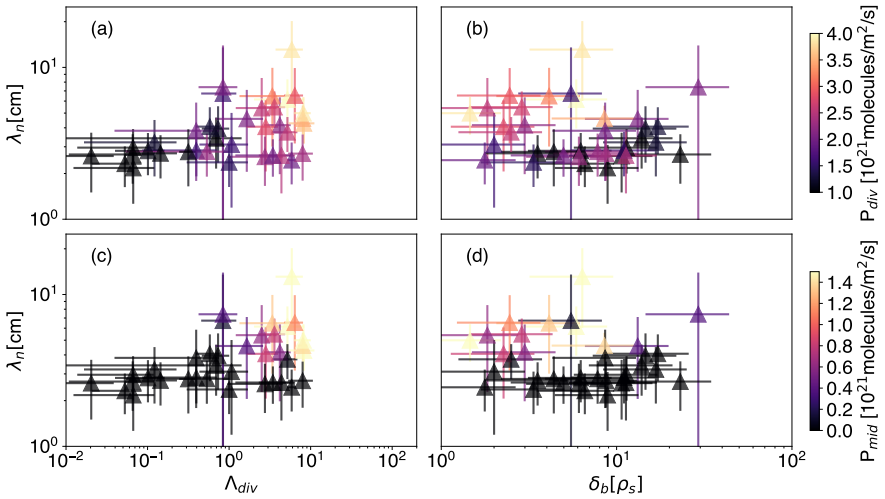

FIG. 11: (a) e-folding length at $\rho \approx 1.4$ as a function of divertor collisionality(b) e-folding length as a function of blob-size. The color refers to the value of sub-divertor neutral pressure. Panel (c) and (d) same as panel (a) and (b) but the color code refers to midplane neutral pressure. Only ASDEX-Upgrade data are presented.

gated in these shots. The results concerning the relation with inter-ELM density profile flattening are summarized in Figure 11 where the e-folding length is shown as a function of divertor collisionality Λ_{div} in panels (a) and (c) and as a function of blob-size in panels (b) and (d). The symbol color code is proportional to the divertor neutral pressure as measured in the subdivertor area in panel (a) and (b), and to the midplane neutral pressure as measured from midplane gauges in panel (c) and (d). From this analysis we can recognize the relation suggested in [4] with increasing λ_n observed when crossing $\Lambda_{div} \approx 1$ even though, as anticipated in [9] the transition is smoother and less clear than in L-Mode. Larger values of Λ_n are obtained at higher neutral pressures (both divertor and midplane), consistently with the constant increase of pressure during the fueling ramp observed in Figure 9. On the other hand from panel (d) we recognize that large blobs are insufficient to ensure the increase of λ_n but for the same blob-size flatter profiles are obtained only for higher values of neutrals at the midplane. Also the relation between e-folding length and blob-size is weaker than in L-Mode thus supporting the idea that the paradigm of filamentary regime transition proposed for the L-Mode need to be revised to provide an unified description of the L and H-mode dynamics.

4 H-MODE FAST PARTICLE PRODUCTION

Electron cyclotron and soft X-ray measurements in the Mega Amp Spherical Tokamak (MAST) have demonstrated that electrons are accelerated to highly supra-thermal energies due to parallel electric fields generated during the eruption of ELM filaments [26]. More recently, the fast ion loss detectors (FILDs) in ASDEX-Upgrade have recorded ion energies well above the primary beam injection energy during ELMs in low density pulses, indicating that energetic ions are being accelerated in these pulses [27]. As in MAST, enhancements in electron cyclotron emission (ECE) and soft X-ray emission were recorded at the start of some of these ELMs, suggesting strongly that electrons were accelerated as well as beam ions. Particles accelerated as a result of ELM filament eruption are expected to be transported rapidly to the SOL, and may contribute significantly to the fluxes of energy and particles impacting on the divertor. It is therefore important to consider the possible impact of these particles on filamentary transport and target heat loads also at different densities. Other things being equal, higher density implies higher collisionality and hence, for a given parallel electric field, a smaller fraction of accelerated electrons. However short-duration enhancements in soft X-ray emission from the low field side plasma periphery, strongly suggesting energetic electron production, occurred during the high density pulses discussed in the previous section.

Figure 12 shows an example of this from shot 34278. Spikes of emission in some edge-localised ECE channels were detected at the same time as the soft X-ray emission enhancements. No clear evidence was found of beam ion acceleration from FILD in these scenarios. Nevertheless, the evidence of energetic electron production in Figure 12 suggests that this phenomenon is common to all H-mode regimes in ASDEX-Upgrade. The quantitative impact of these particles on divertor heat loads remains to be evaluated.

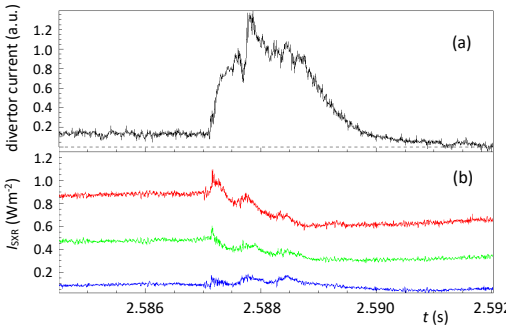

FIG. 12: (a) Divertor shunt current during a Type-I ELM (b) SXR signals from 3 different channels

5 CONCLUSIONS

A unified effort within the EUROfusion Medium-Size-Tokamaks (MST1) Work programme has been coordinated to explore the role of filamentary transport in high density tokamak regimes both in L and H-mode, particular focusing on the issue of *SOL shoulder formation*. Comparable current scans at constant toroidal field or constant q_{95} have been performed to disentangle the role of plasma current from the modification of parallel connection length. It has been shown that the Greenwald fraction determines the onset of shoulder formation both in AUG and TCV whenever the toroidal field is kept constant, reconciling the behavior at different currents. Furthermore, in analogy with JET, shoulder formation coincides with the transition to a high recycling regime for AUG, and conincides with a movement of D_α radiation in the LFS SOL region, as reported in [19] for JET Horizontal Target plasmas. On the other hand TCV, with its complete open divertor, exhibits a different divertor dynamical behavior, with the target density increasing almost linearly with fueling: we have clearly proved that upstream profiles are modified only after peak target density roll-over. The lack of detachment at lower currents during the constant q_{95} scan prevents upstream variation and the development of SOL density profile shoulder. In L-Mode plasmas, the density e-folding length increases with blob-size independently of the current in all the scans performed on ASDEX-Upgrade, whereas the same relation is weaker for TCV. Analysis of the filaments characteristics in the $\Lambda_{div} - \Theta$ plane suggests that in both TCV and AUG resistive baloning character dominates filamentary dynamics, thus suggesting that the different behavior of the two devices must be due to other mechanisms (e.g. SOL opacity, neutral distribution, neutral compression). H-Mode inter-ELM density shoulders have been obtained in ASDEX-Upgrade, in discharges with high levels of both fueling and seeding. On ASDEX-Upgrade we have clearly demonstrated that neither large divertor collisionality nor large blobs are sufficient to guarantee the shoulder formation but high neutral density, in particular in the midplane region, is mandatory. The reason why this is not confirmed in other device [5] is presently under investigation. Work is presently in progress to extend the H-Mode analysis in TCV, where high density H-Mode in detachment conditions has not yet been achieved even with high values of inter-ELM divertor collisionality. Finally signatures of energetic electron accelleration during ELM eruption have been observed even at higher densities, and study are in progress to assess the importance of energetic particle in the SOL transport.

Acknowledgment

This work has been carried out within the framework of the EUROfusion Consortium and has received funding from the Euratom research and training programme 2014-2018 under grant agreement No 633053. The views and opinions expressed herein do not necessarily reflect those of the European Commission.

REFERENCES

[1] M. Kočan et al., Nucl. Fus. **55**, 033019 (2015).
[2] N. Asakura et al., Journal of Nuclear Materials **241-243**, 559–563 (1997).
[3] B. LaBombard et al., Phys. Plasmas **8**, 2107 (2001).
[4] D. Carralero et al., Phys. Rev. Lett. **115**, 215002 (2015).
[5] F. Militello et al., Nucl. Fusion **56**, 016006 (2016).
[6] N. Vianello et al., Nucl. Fusion **57**, 116014 (2017).
[7] B. LaBombard et al., Journal of Nuclear Materials **241-243**, 149–166 (1997).
[8] J. A. Boedo et al., Physics of Plasmas **8**, 4826–4833 (2001).
[9] D. Carralero et al., Nucl. Fusion **57**, 056044 (2017).
[10] H. W. Müller et al., Journ of Nucl. Mater. **463**, 739–743 (2015).
[11] M. Bernert et al., Plasma Phys. Control. Fus. **57**, 014038 (2014).
[12] T. Eich et al., Nuclear Fusion **58**, 034001 (2018).
[13] C. Theiler et al., Nuclear Fusion **57**, 072008 (2017).
[14] C. Sang et al., Plasma Physics and Controlled Fusion **59**, 025009 (2016).
[15] K. Verhaegh et al., in Proceedings of the 23rd PSI Conference, Princeton (2018).
[16] A. Fil et al., Contributions to Plasma Physics **47**, S203 (2018).
[17] C. K. Tsui et al., Physics of Plasmas **25**, 072506 (2018).
[18] J. R. Myra et al., Physics of Plasmas **13**, 112502 (2006).
[19] A. Wynn et al., Nuclear Fusion **58**, 056001 (2018).
[20] F. Militello et al., Nuclear Fusion **56**, 104004 (2016).
[21] A. Andersen, Ultrasonic Imaging **6**, 81–94 (1984).
[22] F. Reimold et al., Nuclear Materials and Energy **12**, 193–199 (2017).
[23] S. Potzel et al., Journal of Nuclear Materials **463**, 541–545 (2015).
[24] D. Carralero et al., Nuclear Fusion **54**, 123005 (2014).
[25] D. Carralero et al., Nuclear Fusion **58**, 096015 (2018).
[26] S. J. Freethy et al., Physical Review Letters **114**, 125004 (2015).
[27] J. Galdon-Quiroga et al., Physical Review Letters **121**, 025002 (2018).